Journal of Integrative Neuroscience

J. Integr. Neurosci. **2026**; 25(8): 50729
https://doi.org/10.31083/JIN50729

Original Research

Gray Matter Volume and Intrinsic Timescale and Their Spatial Coupling Alterations in the Brains of Preterm Infants

Yingxing Zhang[1], Ya Wang[1], Yuchan Liu[2], Jian Zhang[1,*]

[1]Department of Child Healthcare, Anhui Provincial Children's Hospital, 230022 Hefei, Anhui, China
[2]Department of Radiology, Anhui Provincial Children's Hospital, 230022 Hefei, Anhui, China
*Correspondence: zjnetmail@126.com (Jian Zhang)
Academic Editor: Bettina Platt
Submitted: 5 February 2026 Revised: 23 April 2026 Accepted: 29 April 2026 Published: 26 August 2026

Abstract

Background: Extensive neuroimaging abnormalities in multiple brain regions constitute the neural basis of preterm infants (PTIs). However, the function of the brain and its spatial coupling with brain structure remain unknown, leaving a considerable gap in understanding the neural mechanism underlying atypical neurodevelopment in PTIs. **Methods:** Combining structural magnetic resonance imaging (MRI) and resting-state functional magnetic resonance imaging (fMRI) data from 14 PTIs and 14 term infants (TEIs), we quantified gray matter volume (GMV) via voxel-based morphometry, estimated intrinsic timescales from fMRI signals via autocorrelation function (ACF) analysis, and further assessed spatial structure-function coupling across individuals. **Results:** PTIs exhibited GMV alterations in multiple brain regions encompassing high-order cortical and subcortical regions ($p < 0.001$, corrected by family-wise error (FWE)), which were significantly associated with clinical variables such as gestational age ($R = 0.716$, $p < 0.0001$), postnatal age ($R = –0.698$, $p < 0.0001$) and birth weight ($R = 0.727$, $p < 0.0001$). Alterations in intrinsic timescales were revealed at both the spatial distribution (voxel-level $p < 0.001$, Gaussian random field (GRF)-corrected $p < 0.05$) and local regional levels, highlighting functional alterations of the medial frontal gyrus in PTIs (voxel-level $p < 0.001$, GRF-corrected $p < 0.05$). Furthermore, alterations in spatial structure–function coupling were also found in both high-order cortical and subcortical regions, with ACF decay in these regions significantly correlated with serum iron levels ($R = –0.664$, $p = 0.0096$) in PTIs. **Conclusions:** These findings suggest that preterm birth–related neurodevelopmental alterations may be associated with differences in the coordination between brain structure and function, which could be related to variations in neurobehavioral outcomes, and indicate that neuroimaging may provide useful insights into early neurodevelopmental differences in PTIs.

Keywords: preterm infants; structural MRI; functional MRI; neuroimaging; neurodevelopment

1. Introduction

Globally, the annual number of preterm births—defined as delivery before 37 weeks of gestation—exceeds 13.4 million, representing a significant global health challenge and one of the leading causes of mortality in children under five years of age [1]. Additionally, its short-term and long-term effects are strongly associated with poor health, intellectual disabilities and even early onset of chronic disorders, resulting in severe shortages of medical resources, especially in developing countries [2,3]. All of these health issues can directly impact the brain development of preterm infants (PTIs), predisposing them to long-lasting structural and functional alterations that may persist into adolescence, adulthood and even throughout life [4,5,6]. Consequently, characterizing alterations in brain structure, function and spatial coupling in PTIs is imperative, as this understanding is fundamental for developing targeted neural intervention strategies for this vulnerable population.

Structural magnetic resonance imaging (MRI) studies on a neurological basis have revealed that regional brain volume reduction occurs at term-equivalent ages of PTIs, including in the gray matter in both cortical and subcortical regions, white matter and brainstem, as well as in combination with an increase in cerebrospinal fluid (CSF) [7,8]. Moreover, reduced anatomical volumes (particularly in regions such as the thalamus) and cortical curvature and increased surface areas not only have been shown to be associated with cognitive outcomes, movement assessments and neurological examinations at term equivalent age but also serve as crucial predictors of later neurodevelopmental outcomes [8,9,10,11]. Furthermore, resting-state functional magnetic resonance imaging (rs-fMRI) studies have revealed atypical patterns of functional connectivity in the PTIs brain and its relationships with social, sensory, and repetitive behaviors. These identified features can be used to quantify the symptoms of autism, highlighting the effects of preterm birth on functional development [12]. Other studies in which rs-fMRI was integrated with structural MRI and diffusion tensor imaging (DTI) revealed, via advanced computational models, that the contribution of gray and white matter structures to functional connectivity appears to be diminished in the brains of PTIs, potentially forming the neural basis of their long-term neurodevelop-

mental differences [13,14]. Nevertheless, the underpinnings of structure-function coupling require further clarification in PTIs.

Voxel-based morphometry (VBM) is a common method used to study cranial brain structure, allowing the calculation of voxelwise differences in local gray matter volume (GMV) [15,16]. By combining structural MRI data with corresponding behavioral or clinical data, researchers can elucidate the behavior-related underpinnings in healthy brains and associations between GMV alterations and clinical symptoms in diseased brains [17,18]. On the other hand, rs-fMRI can be used to analyze multiple functional indices [19,20,21], such as functional connectivity (FC), regional homogeneity (ReHo), and the amplitude of low-frequency fluctuations (ALFF), to elucidate the neural mechanisms underlying the cognitive behaviors of PTIs [22,23,24]. The autocorrelation function (ACF) has recently become a prevalent approach for studying intrinsic timescales from blood oxygen level-dependent (BOLD) signals, allowing researchers to characterize the temporal window of neural responses in the human brain [25], which may reflect the evolving temporal properties of brain function during development. However, most existing studies focus solely on structural abnormalities or functional anomalies and overlook the synchrony of neural response and structure-function coupling in brain PTIs.

This study integrated the VBM and ACF methods to characterize brain structure and function in a cohort of preterm and term infants (TEIs). We aimed to identify clinically meaningful patterns of GMV reduction and aberrant intrinsic timescales in PTIs, together with associated spatial correlation abnormalities, and to evaluate their associations with key clinical variables, including gestational and postnatal age, birth weight and serum iron levels (Fig. 1). We hypothesized that PTIs exhibit clinically relevant abnormalities in GMV and intrinsic timescales, as well as distinct spatial structure–function patterns, suggesting that neuroimaging may provide useful insights into early atypical neurodevelopment in PTIs.

2. Materials and Methods

2.1 Study Design

The present study explored alterations in the GMV and brain function of PTIs compared with those of TEIs, investigated their clinical relevance, and finally revealed whether structure-function coupling is altered in PTIs by performing three steps of analyses (Fig. 1). In step 1, we used the VBM approach to estimate the GMV from 3D high-resolution MRI of both the PTIs and TEIs (Fig. 1A). In step 2, we calculate the intrinsic timescales by performing a voxelwise ACF analysis of the BOLD signal (Fig. 1B). In step 3, we used spatial structure-function coupling analysis to determine the relationships between GMV and ACF decay for both the PTIs and TEIs (Fig. 1C). We used the STROBE reporting guideline to draft this manuscript, and the STROBE reporting checklist when editing, included in **Supplementary Material**.

2.2 Participants

A total of 23 PTIs and 21 TEIs were recruited from the pediatric department of Anhui Provincial Children's Hospital. All participants were classified into PTIs and TEIs according to gestational age. PTIs were defined as those born before 37 completed weeks of gestation, whereas TEIs were defined as those born at or after 37 completed weeks of gestation. For both the PTI and TEI groups, the gestational age, postnatal age, birth weight, and serum iron level of each infant were recorded. To ensure comparable developmental timing between the two groups, the PTI infants underwent MRI scanning at term-equivalent ages.

Strict inclusion and exclusion criteria were applied to ensure data quality and reliability. The inclusion criteria were as follows: (1) PTIs born at a gestational age <37 weeks or TEIs born at 37–42 weeks; (2) complete clinical information, including gestational age, birth weight, and postnatal age at scan; (3) successful acquisition of both high-quality structural MRI and resting-state fMRI data; and (4) stable clinical condition at the time of MRI examination. The exclusion criteria included the following: (1) major brain abnormalities detected on MRI (e.g., intraventricular hemorrhage grade III–IV, cystic periventricular leukomalacia, or congenital brain malformations); (2) severe motion artifacts or poor image quality that precluded reliable preprocessing or analysis; (3) incomplete imaging data or missing key clinical variables; and (4) significant neonatal complications that may affect brain development [26,27] (e.g., hypoxic-ischemic encephalopathy, intracranial infection, hypoglycemic encephalopathy, or Kernicterus). After the quality control procedures were performed, 14 PTIs and 14 TEIs were included in the final analysis (Fig. 2).

Notably, the difference in postnatal age between groups reflects the study design aimed at matching postmenstrual age at the time of MRI scanning, thereby aligning overall developmental timing from the fetal period to the early postnatal period (Table 1). The detailed demographic and clinical information is provided in Table 1.

2.3 MRI Scans

MRI data were acquired via a 3.0-Tesla Philips Ingenia CX scanner (Equipment No. 96302808; Serial No. 72539; Philips Healthcare, Best, the Netherlands). High-resolution anatomical images were obtained via a 3D T1-weighted magnetization-prepared rapid gradient echo (MPRAGE) sequence with the following parameters: repetition time (TR) = 6.7 ms, echo time (TE) = 3.0 ms, inversion time (TI) = 900 ms, flip angle = 8°, field of view (FOV) = 220 × 220 mm^2, matrix size = 220 × 220, and 360 slices. rs-fMRI images were acquired via a gradient-echo echo-planar imaging (EPI) sequence with the following parameters: TR = 2000 ms, TE = 30 ms, flip angle = 90°, FOV = 100 ×

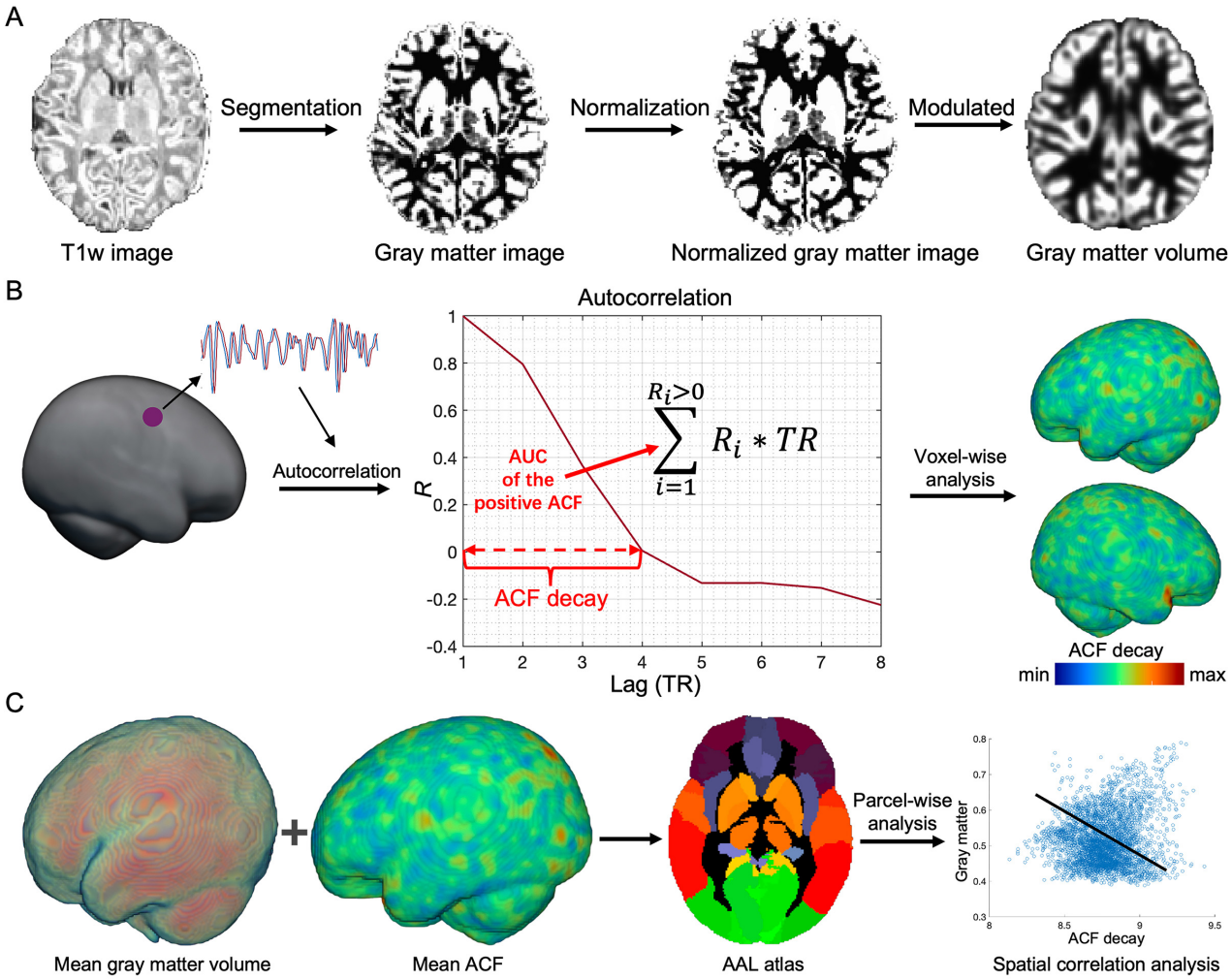

Fig. 1. Study overview. (A) Voxel-based morphometry approach to estimate the gray matter volume (GMV) for each participant. (B) The intrinsic timescale measurement. The intrinsic timescales were calculated from the blood oxygen level-dependent (BOLD) signal by performing a voxelwise autocorrelation function (ACF) analysis. ACF decay was defined as the area under the curve of the positive ACF, which sums the positive values of ρ up to the point where it first crosses zero or becomes negative. (C) Spatial correlation analysis between GMV and ACF decay maps. First, the mean GMV and ACF were calculated across individuals for both the preterm infants (PTIs) and term infants (TEIs). Spatial correlation analysis between the mean GMV and ACF was subsequently performed for each subregion. The subregion was defined via a widely used infant Anatomical Automatic Labeling (AAL) atlas.

Table 1. Demographic and clinical data of PTIs and TEIs.

	PTIs	TEIs	T value	*p* value
Number	14 (7 male)	14 (8 male)	-	-
Gestational age (weeks)	31.36 ± 3.35	39.05 ± 1.38	–7.94	<0.001
Postnatal age (weeks)	9.19 ± 5.36	1.21 ± 0.68	5.52	<0.001
Birth weight (kg)	1.48 ± 0.67	3.32 ± 0.43	–8.63	<0.001
Serum iron (μmol/L)	15.5 ± 10.2	16.24 ± 5.69	–0.24	0.815

100 mm^2, matrix size = 66 × 66, slice thickness = 3 mm, slice number = 36, and a total of 180 volumes. All the infants were scanned under sedation with chloral hydrate (Approval No. H20210013; Tefeng Pharmaceutical Co., Ltd., Nanjing, Jiangsu, China) (dosage: 20 mg/kg) using a standardized protocol. To minimize noise exposure, earmuffs were applied during scanning. Throughout the data acquisition, a neonatal nurse continuously monitored the arterial oxygen saturation and heart rate of each infant, and the MRI scan was immediately discontinued if any unexpected events occurred.

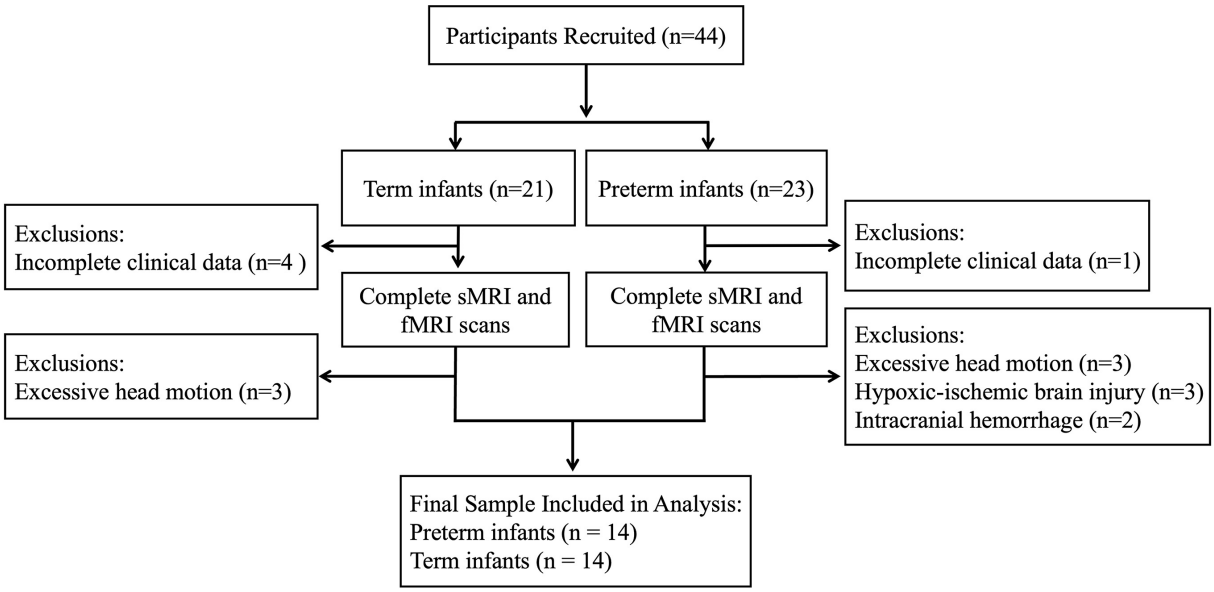

Fig. 2. Study participant enrollment and exclusion procedures. A total of 44 infants were initially recruited, including 23 preterm infants and 21 term infants. Participants with incomplete clinical data, excessive head motion during MRI scanning, hypoxic-ischemic brain injury, or intracranial hemorrhage were excluded according to the predefined criteria. After quality control and eligibility assessment, 14 preterm infants and 14 term infants with complete structural MRI and fMRI data were included in the final analyses.

2.4 Data Preprocessing

The VBM analysis using FMRIB Software Library (FSL) was carried out in accordance with the methodology reported in a previous study [28]. Specifically, structural data were analyzed with the FSL-VBM pipeline [15,16], which uses FSL tools (https://web.mit.edu/fsl_v5.0.10/fsl/doc/wiki/FSL.html) to calculate the GMV for each infant. 3D MR images were first skull-stripped using Brain Extraction Tool (BET) [29]. All skull-stripping results were visually inspected to ensure accurate brain extraction. Next, brain tissue segmentation was implemented via FMRIB's Automated Segmentation Tool (FAST) [30], which divides the brain into gray matter, white matter and cerebrospinal fluid. The individual gray matter image was subsequently aligned to a widely used infant template [31] (University of North Carolina (UNC) Infant Atlas: neonates) via the registration command FMRIB's Linear Image Registration Tool (FLIRT), followed by nonlinear registration via FMRIB's Non-linear Image Registration Tool (FNIRT) [32]. Owing to the indistinct gray–white matter boundary in the infant brain, tissue segmentation may be imperfect, which could influence the accurate separation of gray and white matter. Here, the segmentation and normalization results were carefully evaluated through visual inspection to minimize potential misclassification and ensure accurate spatial alignment, which is consistent with previous infant VBM studies [28]. The normalized GMV images were further modulated to correct for local expansion or contraction by dividing by the Jacobian of the warp field. Finally, the modulated images were smoothed with an isotropic Gaussian kernel with a sigma of 2 mm.

The resting-state fMRI images were preprocessed via a combination of analysis packages [33], including the FSL(https://fsl.fmrib.ox.ac.uk/fsl/docs/) and Analysis of Functional NeuroImages (AFNI) (https://afni.nimh.nih.gov/). First, we discarded the first 10 volumes to allow for signal stabilization and T1 relaxation effects, followed by slice-timing correction to adjust for interslice acquisition delays. Second, head motion correction was performed by realigning all functional volumes to the first volume, after which the realigned functional images were coregistered to the corresponding high-resolution anatomical images and subsequently normalized to a widely used infant template. Head motion was carefully controlled during preprocessing. Framewise displacement (FD) was calculated to quantify motion, and subjects with excessive motion (mean FD >0.2 mm) were excluded on the basis of predefined criteria [34,35]. No significant group differences in mean FD were observed. Third, the functional images were resampled to isotropic voxel sizes of $2 \times 2 \times 2$ mm^3. Fourth, spatial smoothing was applied to resampled images with a 4-mm full-width at half-maximum (FWHM) Gaussian kernel. Next, linear detrending was performed to eliminate the linear drift of the fMRI signal. Finally, nuisance regression was applied to remove the effects of six head motion parameters as well as white matter and cerebrospinal fluid signals, followed by temporal bandpass filtering (0.01–0.1 Hz).

2.5 ACF Analysis

The intrinsic timescale of the BOLD signal, reflecting the temporal window of the neural response, is measured via the ACF approach, which generates an ACF decay index

[25]. The ACF measures the correlation of a time series with itself at different time lags. For a given fMRI time series x_t (t = 1, 2, …, T, where T is the number of time points), its mean is defined as follows:

$$\bar{x} = \frac{1}{T}\sum_{t=1}^{T} x_t$$

The ACF at lag k is then defined as follows:

$$\rho(k) = \frac{\sum_{t=1}^{T-k}(x_t - \bar{x})(x_{t-k} - \bar{x})}{\sum_{t=1}^{T}(x_t - \bar{x})^2}, k = 0, 1, 2, \ldots$$

where $\rho(0)=1$ indicates that the autocorrelation at zero lag is always 1 after normalization and where $\rho(k)$ describes the similarity between the signal and its lagged version at time shift k. Here, the ACF decay was defined as the area under the curve of the positive ACF [36], which is the sum of the positive values of ρ up to the point where it first crosses zero or becomes negative (Fig. 1B). A larger sum indicates a longer ACF decay. A smaller ACF decay indicates that brain regions with faster timescales tend to respond quickly to external stimuli or information, whereas those with greater ACF decay (slower timescales) integrate information over longer periods. The procedures for ACF analysis were carried out with an in-house MATLAB code (The MathWorks, Inc., Natick, MA, USA).

2.6 Spatial Structure-Function Coupling Analysis

Structure–function coupling at both the group and individual levels was assessed using Spearman correlation between the GMV and ACF decay maps. At the group level, first, GMV and ACF decay images were averaged across individuals within the PTIs and TEIs, respectively, yielding mean GMV and ACF maps for each group. Second, these mean maps were parcellated into multiple brain regions via the infant AAL atlas, and Spearman correlations between GMV and ACF decay were computed for each subregion. Finally, differences in spatial correlations between the PTIs and TEIs were assessed via a random permutation test (N = 10,000 times). To control for multiple comparisons, significance levels were further corrected via the Benjamini-Hochberg false discovery rate (FDR) method.

At the individual level, the individual GMV and ACF decay maps were parcellated into multiple brain regions via the infant AAL atlas, and Spearman correlations between GMV and ACF decay were computed for each subregion. Group differences in structure–function coupling between the PTIs and TEIs were assessed via a two-sample t test.

2.7 Statistical Analyses

Given the significant between-group differences (e.g., group differences in GMV and ACF) in gestational age, postnatal age, and birth weight, these variables were carefully considered in the statistical analyses. Gestational age and postnatal age were included as covariates to account for differences in developmental timing, which may influence brain maturation. Birth weight, which is closely related to prematurity, was considered a potential confounding factor; however, its inclusion as a covariate was carefully evaluated to avoid overadjustment. This approach aimed to balance the need to control for confounding effects while preserving meaningful group-related differences. Group differences in GMV between the PTIs and TEIs were assessed via permutation-based nonparametric testing with 5000 random permutations. The significance threshold was set at $p < 0.001$, and the threshold-free cluster enhancement method with family-wise error (FWE) correction was used for multiple comparisons. The case-control group differences in ACF decay were evaluated via two-sample t tests. For the regional ACF decay map, the significance threshold was set to $p < 0.001$ at the voxel level, followed by Gaussian random field (GRF) correction at the cluster level of $p < 0.05$. The differences in the global spatial distribution of the ACF decay were investigated via two-sample t tests, with the significance levels corrected via the Benjamini-Hochberg false discovery rate (FDR).

The voxelwise relationships between GMV (within regions showing significant group differences in GMV) and clinical variables—including gestational age, postnatal age, birth weight, and serum iron level—were assessed across all infants via Pearson correlation analysis. The group differences in spatial correlations between the PTIs and TEIs were assessed via a random permutation test (N = 10,000 times). Within each group, the associations between ACF decay and serum iron levels were evaluated using Pearson correlation analysis. The statistical significance of the above results was further corrected for multiple comparisons using the Benjamini–Hochberg FDR for multiple comparisons.

3. Results

3.1 Alterations in GMV in PTI Infants

The between-group statistical comparisons revealed that the GMVs of the thalamus, medial orbital frontal gyrus (MOFG), supplementary motor area (SMA), and putamen in the PTIs were significantly lower than those in the TEIs (Fig. 3A, $p < 0.001$, corrected by FWE). Moreover, the results of the voxelwise Pearson correlation analysis revealed that decreased GMV was positively correlated with gestational age (Fig. 3B, **Supplementary Fig. 1A**) and birth weight (Fig. 3C, **Supplementary Fig. 1B**) and negatively correlated with postnatal age (Fig. 3D, **Supplementary Fig. 1C**) across all the infants. The mean GMV in these regions also showed similar relationships with gestational age (Fig. 3B, $R = 0.716$, $p < 0.0001$), birth weight (Fig. 3C, $R = 0.727$, $p < 0.0001$) and postnatal age (Fig. 3D, $R = –0.698$, $p < 0.0001$).

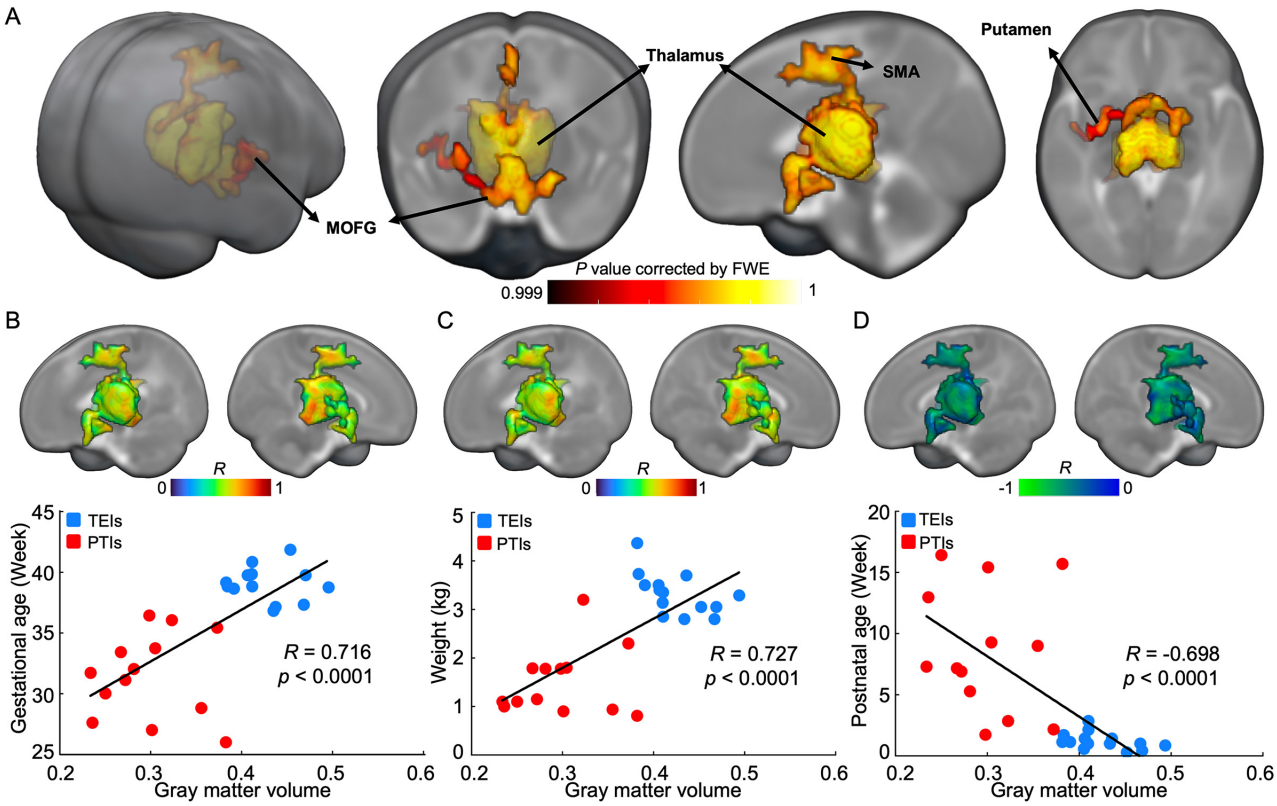

Fig. 3. Statistical comparisons of GMV. (A) Voxelwise statistical comparisons between the PTIs and TEIs. The statistical significance level was set as $p < 0.001$ after multiple comparisons were corrected by the threshold-free cluster enhancement method with family-wise error (FWE). Relationships between GMV and clinical variables, such as gestational age (B), weight (C) and postnatal age (D), are shown. The top part of the graph shows the results of the voxelwise Pearson correlation analysis between GMV and clinical variables across all the infants, and the correlation significance level was corrected by the Benjamini-Hochberg false discovery rate (FDR). The bottom part of the graph shows the correlations between the mean GMV and clinical variables across all infants. MOFG, medial orbital frontal gyrus; SMA, supplementary motor area.

3.2 Alterations in ACF Decay in the PTIs

A previous study reported that ACF decay has a hierarchical organization in the adult brain [25]. Unlike in the adult brain, ACF decay in the newborn infant brain is not in line with this principle (Fig. 4A), possibly because their functional networks are not yet differentiated. The histogram demonstrated a significant difference in the spatial distribution between the PTIs and TEIs, with the most pronounced difference observed in the ACF decay values between 8.5 and 9 (Fig. 4B, $p < 0.001$). The case-control group difference analysis revealed that the ACF decayed in the left medial frontal gyrus (MFG. L) was significantly greater in the TEIs than in the PTIs (Fig. 4C, voxel-level $p < 0.001$, GRF-corrected $p < 0.05$).

3.3 Abnormalities in Structure-Function Coupling in PTIs

At the group level, spatial correlations in multiple brain regions, such as the left Heschl's gyrus (HES. L), $R_{Diff} = 0.417$, FDR <0.0001) and right Heschl's gyrus (HES. R), $R_{Diff} = 0.589$, FDR <0.0001) in the PTIs were significantly greater than those in the TEIs (Fig. 5A and **Supplementary Table 1**). However, the left anterior cingulum (ACG. L), $R_{Diff} = 0.432$, FDR <0.0001), left middle cingulum (MCG. L), $R_{Diff} = 0.406$, FDR <0.0001), left amygdala (AMYG. L), $R_{Diff} = 0.345$, FDR = 0.0045) and left caudate (CAU. L), $R_{Diff} = 0.476$, FDR <0.0001) exhibited significantly lower spatial correlations in the PTIs than in the TEIs (Fig. 5C and **Supplementary Table 1**). At the individual level, significant differences in structure-function coupling (**Supplementary Table 2**) between the two groups were also observed in the MCG. L ($p_{uncorrected} = 0.0326$), HES. R ($p_{uncorrected} = 0.0351$) and CAU. L ($p_{uncorrected} = 0.0292$).

Importantly, the mean ACF decay in regions showing greater spatial correlations in the PTIs was significantly and negatively associated with serum iron ($R = –0.664$, $p = 0.0096$; Fig. 5B), whereas no such relationship was observed in the TEIs ($R = 0.1014$, $p = 0.7301$; Fig. 5B). Moreover, no significant associations were observed in either PTIs or TEIs between serum iron levels and the mean ACF decay in regions exhibiting lower spatial correlations in the PTIs (Fig. 5D).

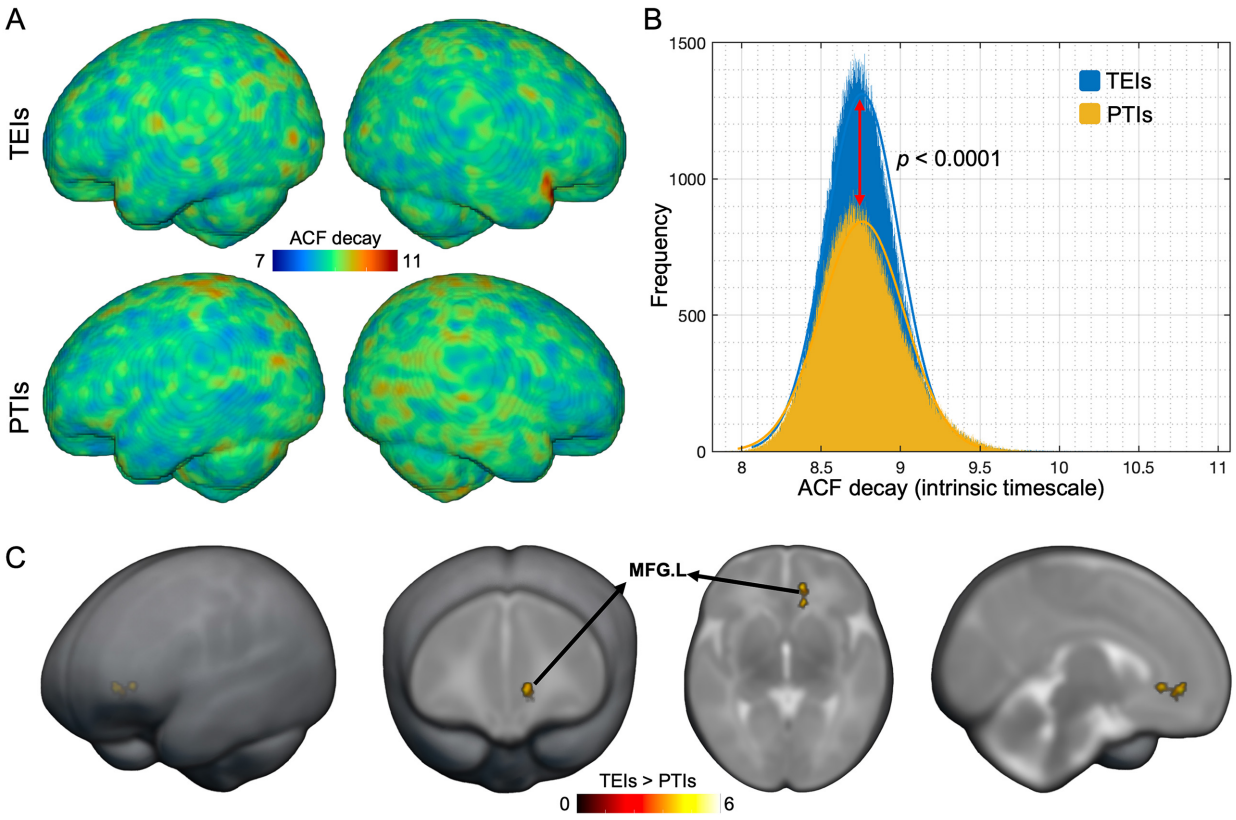

Fig. 4. Statistical comparisons of ACF decay. (A) The mean ACF decay of the PTIs and TEIs. (B) The histogram graph shows the global distribution of ACF decay for the PTIs and TEIs. The ACF decay of the TEIs was significantly greater than that of the PTIs, with the most pronounced difference observed in the ACF decay values between 8.5 and 9. (C) Voxelwise statistical comparisons between the PTIs and TEIs. The statistical significance level was set as a voxel-level $p < 0.001$ and Gaussian random field cluster level-corrected $p < 0.05$. MFG. L, left medial frontal gyrus.

4. Discussion

In this study, we explored regional alterations in GMV and intrinsic timescales and further clarified their spatial relationships to understand how these altered patterns affect brain development in PTIs. We reported three findings in local regions of GMV and ACF decay: (i) PTIs showed significantly reduced GMV across both cortical and subcortical regions, with these reductions significantly associated with clinical variables, such as gestational age, postnatal age and birth weight; (ii) intrinsic timescales were altered, as represented by changes in ACF decay across both spatial distribution and local regional levels; and (iii) abnormal structure–function coupling was observed in PTIs across both cortical and subcortical regions, where ACF decay was significantly associated with serum iron levels.

During the third trimester, both cortical and subcortical gray matter undergo rapid structural and functional maturation, with synaptogenesis, dendritic arborization, and gyrification predominating in the cerebral cortex and substantial volumetric expansion and circuit refinement occurring in subcortical regions such as the thalamus and basal ganglia [37,38]. By disrupting these neurodevelopmental processes, preterm birth leads to reduced GMV in both cortical and subcortical GMVs, potentially underpinning the long-term cognitive and motor deficits observed in PTIs [39,40]. Consistent with prior studies [41,42], the present findings revealed a reduced GMV in the medial orbital frontal gyrus, a region implicated in higher-order cognitive processes [43], as well as in the supplementary motor area, which plays a key role in planning and executing complex movements [44]. Subcortical regions, including the thalamus and putamen, also presented a reduced GMV, suggesting potential disruptions in the cortico-basal ganglia–thalamo–cortical circuit, which is crucial to coordinated cognitive and motor behaviors [45]. More importantly, alterations in GMV were positively associated with gestational age and birth weight but negatively associated with postnatal age, indicating that earlier preterm birth is linked to slower development of both cortical and subcortical GMV. Together, these findings provide evidence that disruptions in neurodevelopmental processes during both the perinatal and postnatal periods may lead to lasting impairments in cognitive and motor function in PTIs.

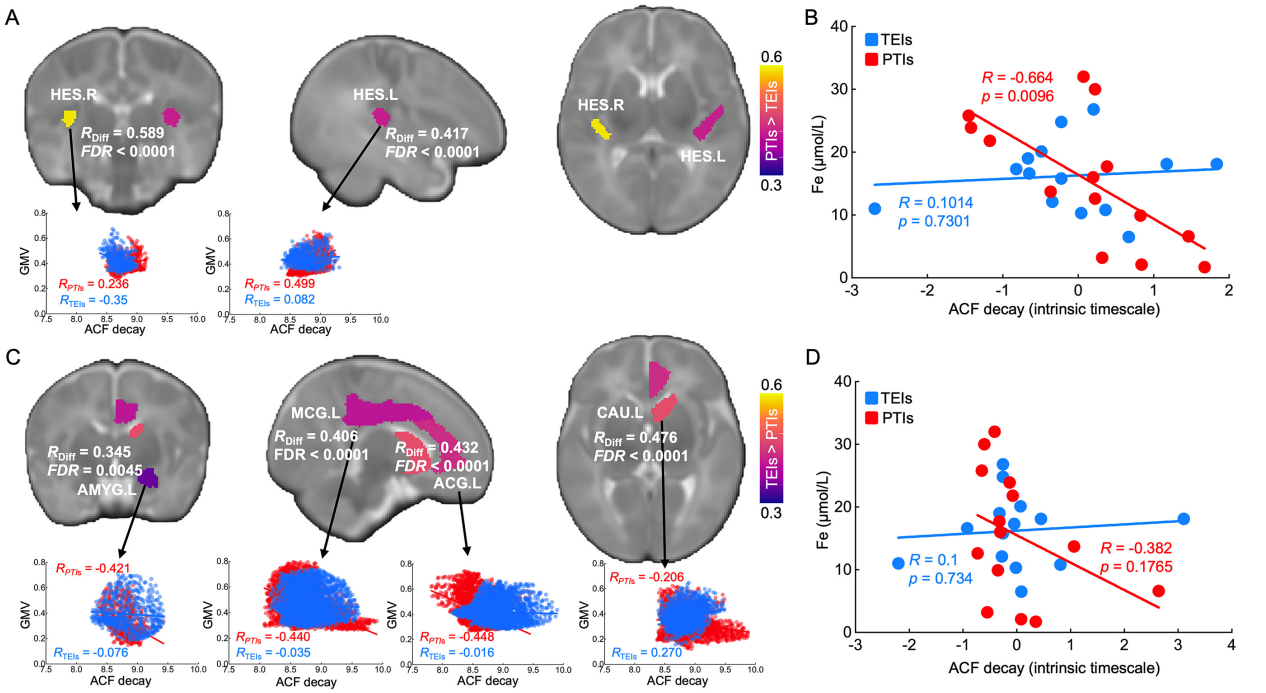

Fig. 5. Statistical differences in structure-function coupling at group level. (A) The spatial correlations in brain regions are significantly greater in PTIs than in TEIs. Scatter plots represent the spatial correlations between ACF decay and GMV in either PTIs or TEIs. (B) Relationships between mean ACF decay in regions with greater spatial correlation between PTIs and serum iron. (C) The spatial correlations in brain regions are significantly lower in PTIs than in TEIs. (D) Relationships between mean ACF decay in regions with lower spatial correlations between PTIs and serum iron. The group differences in spatial correlations between the PTIs and TEIs were assessed via a random permutation test (N = 10,000 times), and the significance levels were corrected via the Benjamini-Hochberg FDR. HES. L, left Heschl's gyrus; HES. R, right Heschl's gyrus; ACG. L, left anterior cingulum; MCG. L, left middle cingulum; AMYG. L, left amygdala; CAU. L, left caudate.

An intrinsic timescale has been proposed to capture temporal characteristics of neural responses [46], a process that critically depends on an intact brain structure [47]. In the present study, we observed significant differences in the spatial distribution of ACF decay between PTIs and TEIs, potentially indicating maturational delay and altered neural synchrony in PTIs [25]. Notably, the case-control group analysis revealed significant regional differences in ACF decay between the two groups, which were primarily localized to the left medial frontal gyrus. This region is implicated in higher-order functions such as decision-making [48], emotion regulation [49], and social cognition [50], suggesting that functional alterations in this area may contribute to atypical maturation of cognitive function in PTIs. In addition, we found abnormalities in structure-function coupling distributed across both higher-order cortical regions in PTIs, such as the Heschl's gyrus and cingulate gyrus, and subcortical regions, including the caudate and amygdala. The interpretation of increased versus decreased structure–function coupling remains complex, particularly in the context of early brain development. From a developmental perspective, brain maturation is characterized by a gradual transition from locally organized networks to more distributed and specialized systems, accompanied by increased network segregation and efficient integration [51,52]. Within this framework, alterations in structure–function coupling may reflect different underlying neurodevelopmental processes. Specifically, increased coupling observed in certain regions (e.g., the Heschl's gyrus) may indicate a state of immature network organization, in which functional activity remains more tightly constrained by underlying structural properties because of limited functional specialization [53]. In contrast, decreased coupling in regions such as the cingulate cortex, amygdala, and caudate may suggest disrupted integration between structure and function, potentially reflecting impaired coordination across distributed brain systems. These regions are known to play critical roles in higher-order cognitive and affective processing, and their altered coupling may indicate early deviations in the development of large-scale brain networks [54,55]. Collectively, these findings suggest that preterm birth may be associated with an imbalance in the maturation of network segregation and integration, leading to heterogeneous patterns of structure–function coupling across brain regions in PTIs.

Importantly, ACF decay in brain regions with aberrant structure-function coupling was negatively correlated with serum iron concentration in PTIs, whereas no such relationship was observed in TEIs. Iron plays a critical role in early brain development, particularly in processes such as myelination and cellular metabolism. It is essential for oligodendrocyte function and the formation of myelin, which in turn influences neural signal transmission. In addition, emerging evidence suggests that iron may also be involved in the maturation of the blood–brain barrier (BBB), contributing to the regulation of the neural microenvironment [56,57,58]. Disruptions in iron homeostasis during early life may therefore affect both structural and functional brain development. In this context, the observed association between the intrinsic timescale and serum iron concentration may reflect alterations in neurodevelopmental processes; however, this relationship should be interpreted cautiously and warrants further investigation.

An important consideration in the present study is the difference in postnatal age between PTIs and TEIs. This difference arises from the study design, which aimed to align postmenstrual age at the time of MRI scanning, thereby matching the overall developmental timing from the fetal period to the early postnatal period. While this approach is typically used in neonatal neuroimaging to ensure comparability in the maturational stage, it also introduces differences in postnatal experience between groups. Notably, PTIs undergo a longer period of extrauterine exposure prior to scanning, which may influence both structural and functional brain development [55,59]. Early postnatal experience, including sensory stimulation, medical care, and environmental factors, has been shown to shape brain maturation during this critical period [59]. Therefore, the observed group differences may reflect not only the intrinsic effects of prematurity but also the influence of postnatal environmental exposure. These findings should thus be interpreted within a developmental framework that considers the distinction between postmenstrual age (as an index of maturational timing) and postnatal age (as an index of environmental exposure) [60]. Future studies incorporating longitudinal designs and more detailed characterization of postnatal environments will be important for disentangling these effects and further clarifying their contributions to early brain development.

5. Limitations of Current Research

The findings must be interpreted in the context of potential limitations. First, the relatively small sample size may limit the statistical power of the present study and reduce the robustness of the findings. Although permutation testing and multiple comparison corrections were applied, the risk of both false positives and false negatives cannot be fully excluded. This issue is particularly relevant for correlation analyses with clinical variables, which may be more susceptible to instability in small samples. Therefore, the current findings should be interpreted with caution and require validation in larger, independent cohorts. Second, given the close relationships among prematurity, birth weight, and developmental timing, the covariate strategy may influence the observed results and should be interpreted with caution. In addition, preterm infants constitute a heterogeneous population, and unmeasured factors (e.g., neonatal complications, nutrition, and environmental exposures) may influence brain development. These potential confounders were not fully accounted for and may affect the results; thus, the findings should be interpreted with caution and require validation in larger, well-characterized cohorts. Third, it should be noted that all the infants were scanned under chloral hydrate sedation, which may influence their resting-state functional measures. Finally, future longitudinal studies integrating multiple biological metrics are needed to provide a better understanding of how preterm birth affects neurodevelopment and subsequent neurobehavioral outcomes.

6. Conclusions

This study revealed alterations in GMV across both cortical and subcortical regions in PTIs, which were significantly associated with gestational age, postnatal age, and birth weight and may be related to neurodevelopmental differences. The intrinsic timescale evaluated by ACF decay demonstrated group differences in both spatial distribution and regional levels, suggesting altered temporal characteristics of neural activity in PTIs. Furthermore, differences in structure–function coupling were observed in higher-order cognitive and subcortical regions, where ACF decay was associated with serum iron levels. These findings suggest that preterm birth–related brain development may be associated with variations in the coordination between brain structure and function. Taken together, these results provide preliminary evidence that multimodal neuroimaging combined with clinical and biochemical measures may offer useful insights into early neurodevelopmental variation in PTIs.

Availability of Data and Materials

The datasets generated and analyzed during the current study are available from the corresponding author upon reasonable request.

Author Contributions

YZ and JZ designed the research study, YZ and JZ performed the research, YW and YL provided help and contributed to the experimental design, JZ analyzed the data. All authors contributed to editorial changes in the manuscript. All authors read and approved the final manuscript. All authors have participated sufficiently in the work and agreed to be accountable for all aspects of the work.

Ethics Approval and Consent to Participate

The authors obtained written informed consent from a parent or legal guardian of each infant after providing a detailed explanation of the study. This study was approved by the Ethics Committee of Anhui Provincial Children's Hospital (Reference: EYLL-2023-027) and conformed to the tenets of the Declaration of Helsinki.

Acknowledgment

The authors gratefully acknowledge all the participants whose cooperation and support made this study possible.

Funding

This work was supported by the Health Research Project of Anhui Province, "Prediction of Neurobehavioral Development in Premature Infants Based on Independent Component Analysis of Brain Functional Network Effective Connectivity" [Grant Number AHWJ2022b087].

Conflicts of Interest

The authors declare no conflicts of interest.

Supplementary Material

Supplementary material associated with this article can be found, in the online version, at https://doi.org/10.31083/JIN50729.

References

[1] Ohuma EO, Moller AB, Bradley E, Chakwera S, Hussain-Alkhateeb L, Lewin A, et al. National, regional, and global estimates of preterm birth in 2020, with trends from 2010: a systematic analysis. Lancet (London, England). 2023; 402: 1261–1271. https://doi.org/10.1016/S0140-6736(23)00878-4

[2] Perin J, Mulick A, Yeung D, Villavicencio F, Lopez G, Strong KL, et al. Global, regional, and national causes of under-5 mortality in 2000-19: an updated systematic analysis with implications for the Sustainable Development Goals. The Lancet. Child & Adolescent Health. 2022; 6: 106–115. https://doi.org/10.1016/S2352-4642(21)00311-4

[3] Sarda SP, Sarri G, Siffel C. Global prevalence of long-term neurodevelopmental impairment following extremely preterm birth: a systematic literature review. The Journal of International Medical Research. 2021; 49: 3000605211028026. https://doi.org/10.1177/03000605211028026

[4] De Asis-Cruz J, Andescavage N, Limperopoulos C. Adverse Prenatal Exposures and Fetal Brain Development: Insights From Advanced Fetal Magnetic Resonance Imaging. Biological Psychiatry. Cognitive Neuroscience and Neuroimaging. 2022; 7: 480–490. https://doi.org/10.1016/j.bpsc.2021.11.009

[5] Bethlehem RAI, Seidlitz J, White SR, Vogel JW, Anderson KM, Adamson C, et al. Brain charts for the human lifespan. Nature. 2022; 604: 525–533. https://doi.org/10.1038/s41586-022-04554-y

[6] Brouwer RM, Klein M, Grasby KL, Schnack HG, Jahanshad N, Teeuw J, et al. Genetic variants associated with longitudinal changes in brain structure across the lifespan. Nature Neuroscience. 2022; 25: 421–432. https://doi.org/10.1038/s41593-022-01042-4

[7] Padilla N, Alexandrou G, Blennow M, Lagercrantz H, Ådén U. Brain Growth Gains and Losses in Extremely Preterm Infants at Term. Cerebral Cortex (New York, N.Y. : 1991). 2015; 25: 1897–1905. https://doi.org/10.1093/cercor/bht431

[8] Story L, Davidson A, Patkee P, Fleiss B, Kyriakopoulou V, Colford K, et al. Brain volumetry in fetuses that deliver very preterm: An MRI pilot study. NeuroImage. Clinical. 2021; 30: 102650. https://doi.org/10.1016/j.nicl.2021.102650

[9] Kline JE, Sita Priyanka Illapani V, He L, Parikh NA. Automated brain morphometric biomarkers from MRI at term predict motor development in very preterm infants. NeuroImage. Clinical. 2020; 28: 102475. https://doi.org/10.1016/j.nicl.2020.102475

[10] Kline JE, Illapani VSP, He L, Altaye M, Logan JW, Parikh NA. Early cortical maturation predicts neurodevelopment in very preterm infants. Archives of Disease in Childhood. Fetal and Neonatal Edition. 2020; 105: 460–465. https://doi.org/10.1136/archdischild-2019-317466

[11] Skiöld B, Eriksson C, Eliasson AC, Adén U, Vollmer B. General movements and magnetic resonance imaging in the prediction of neuromotor outcome in children born extremely preterm. Early Human Development. 2013; 89: 467–472. https://doi.org/10.1016/j.earlhumdev.2013.03.014

[12] França LGS, Ciarrusta J, Gale-Grant O, Fenn-Moltu S, Fitzgibbon S, Chew A, et al. Neonatal brain dynamic functional connectivity in term and preterm infants and its association with early childhood neurodevelopment. Nature Communications. 2024; 15: 16. https://doi.org/10.1038/s41467-023-44050-z

[13] Rogers CE, Lean RE, Wheelock MD, Smyser CD. Aberrant structural and functional connectivity and neurodevelopmental impairment in preterm children. Journal of Neurodevelopmental Disorders. 2018; 10: 38. https://doi.org/10.1186/s11689-018-9253-x

[14] Hong Y, Cornea E, Girault JB, Bagonis M, Foster M, Kim SH, et al. Structural and functional connectome relationships in early childhood. Developmental Cognitive Neuroscience. 2023; 64: 101314. https://doi.org/10.1016/j.dcn.2023.101314

[15] Douaud G, Smith S, Jenkinson M, Behrens T, Johansen-Berg H, Vickers J, et al. Anatomically related grey and white matter abnormalities in adolescent-onset schizophrenia. Brain : a Journal of Neurology. 2007; 130: 2375–2386. https://doi.org/10.1093/brain/awm184

[16] Good CD, Johnsrude IS, Ashburner J, Henson RN, Friston KJ, Frackowiak RS. A voxel-based morphometric study of ageing in 465 normal adult human brains. NeuroImage. 2001; 14: 21–36. https://doi.org/10.1006/nimg.2001.0786

[17] Mechelli A, Price CJ, Friston KJ, Ashburner J. Voxel-based morphometry of the human brain: methods and applications. Current Medical Imaging. 2005; 1: 105-113.

[18] Peterson BS, Vohr B, Staib LH, Cannistraci CJ, Dolberg A, Schneider KC, et al. Regional brain volume abnormalities and long-term cognitive outcome in preterm infants. JAMA. 2000; 284: 1939–1947. https://doi.org/10.1001/jama.284.15.1939

[19] Zang Y, Jiang T, Lu Y, He Y, Tian L. Regional homogeneity approach to fMRI data analysis. NeuroImage. 2004; 22: 394–400. https://doi.org/10.1016/j.neuroimage.2003.12.030

[20] van den Heuvel MP, Hulshoff Pol HE. Exploring the brain network: a review on resting-state fMRI functional connectivity. European Neuropsychopharmacology : the Journal of the European College of Neuropsychopharmacology. 2010; 20: 519–534. https://doi.org/10.1016/j.euroneuro.2010.03.008

[21] Zou QH, Zhu CZ, Yang Y, Zuo XN, Long XY, Cao QJ, et al. An improved approach to detection of amplitude of low-frequency fluctuation (ALFF) for resting-state fMRI: fractional ALFF. Journal of Neuroscience Methods. 2008; 172: 137–141. https://doi.org/10.1016/j.jneumeth.2008.04.012

[22] Lee W, Morgan BR, Shroff MM, Sled JG, Taylor MJ. The de-

velopment of regional functional connectivity in preterm infants into early childhood. Neuroradiology. 2013; 55 Suppl 2: 105–111. https://doi.org/10.1007/s00234-013-1232-z

[23] Damera SR, De Asis-Cruz J, Cook KM, Kapse K, Spoehr E, Murnick J, et al. Regional homogeneity as a marker of sensory cortex dysmaturity in preterm infants. iscience. 2024; 27: 109662. https://doi.org/10.1016/j.isci.2024.109662

[24] Feng Y, Wang Y, Li X, Dai L, Zhang J. Differences in the amplitude of low-frequency fluctuations of spontaneous brain activity between preterm and term infants. Frontiers in Neurology. 2024; 15: 1346632. https://doi.org/10.3389/fneur.2024.1346632

[25] Raut RV, Snyder AZ, Raichle ME. Hierarchical dynamics as a macroscopic organizing principle of the human brain. Proceedings of the National Academy of Sciences of the United States of America. 2020; 117: 20890–20897. https://doi.org/10.1073/pnas.2003383117

[26] Liu Y, Feng Y, Guo Y, Chen J, Liu C, Liang J. Clinical predictors of poor outcome of bacterial meningitis in infants less than 90 days: a systematic review. Frontiers in Pediatrics. 2024; 12: 1414778. https://doi.org/10.3389/fped.2024.1414778

[27] van Laerhoven H, de Haan TR, Offringa M, Post B, van der Lee JH. Prognostic tests in term neonates with hypoxic-ischemic encephalopathy: a systematic review. Pediatrics. 2013; 131: 88–98. https://doi.org/10.1542/peds.2012-1297

[28] Deniz Can D, Richards T, Kuhl PK. Early gray-matter and white-matter concentration in infancy predict later language skills: a whole brain voxel-based morphometry study. Brain and Language. 2013; 124: 34–44. https://doi.org/10.1016/j.bandl.2012.10.007

[29] Jenkinson M. BET2: MR-based estimation of brain, skull and scalp surfaces. In Eleventh Annual Meeting of the Organization for Human Brain Mapping (Vol. 17, p. 167). 2005.

[30] Zhang Y, Brady M, Smith S. Segmentation of brain MR images through a hidden Markov random field model and the expectation-maximization algorithm. IEEE Transactions on Medical Imaging. 2002; 20: 45–57. https://doi.org/10.1109/42.906424

[31] Shi F, Yap PT, Wu G, Jia H, Gilmore JH, Lin W, et al. Infant brain atlases from neonates to 1- and 2-year-olds. PloS One. 2011; 6: e18746. https://doi.org/10.1371/journal.pone.0018746

[32] Andersson J, Jenkinson M, Smith S. Non-linear registration, aka Spatial normalisation FMRIB technical report TR07JA2. FMRIB Analysis Group of the University of Oxford. 2007; 2: e21.

[33] Hu S, Kan H, Kan J, Li C, Yuan A, Xu C, et al. Longitudinal Changes in Functional Connectivity of the Caudate Is Associated With Recovery From Bell's Palsy. Frontiers in Aging Neuroscience. 2019; 11: 295. https://doi.org/10.3389/fnagi.2019.00295

[34] Power JD, Barnes KA, Snyder AZ, Schlaggar BL, Petersen SE. Spurious but systematic correlations in functional connectivity MRI networks arise from subject motion. NeuroImage. 2012; 59: 2142–2154. https://doi.org/10.1016/j.neuroimage.2011.10.018

[35] Van Dijk KRA, Sabuncu MR, Buckner RL. The influence of head motion on intrinsic functional connectivity MRI. NeuroImage. 2012; 59: 431–438. https://doi.org/10.1016/j.neuroimage.2011.07.044

[36] Manea AMG, Zilverstand A, Ugurbil K, Heilbronner SR, Zimmermann J. Intrinsic timescales as an organizational principle of neural processing across the whole rhesus macaque brain. elife. 2022; 11: e75540. https://doi.org/10.7554/eLife.75540

[37] Ball G, Pazderova L, Chew A, Tusor N, Merchant N, Arichi T, et al. Thalamocortical Connectivity Predicts Cognition in Children Born Preterm. Cerebral Cortex (New York, N.Y. : 1991). 2015; 25: 4310–4318. https://doi.org/10.1093/cercor/bhu331

[38] Eyre M, Fitzgibbon SP, Ciarrusta J, Cordero-Grande L, Price AN, Poppe T, et al. The Developing Human Connectome Project: typical and disrupted perinatal functional connectivity. Brain : a Journal of Neurology. 2021; 144: 2199–2213. https://doi.org/10.1093/brain/awab118

[39] Lemola S, Oser N, Urfer-Maurer N, Brand S, Holsboer-Trachsler E, Bechtel N, et al. Effects of gestational age on brain volume and cognitive functions in generally healthy very preterm born children during school-age: A voxel-based morphometry study. PloS One. 2017; 12: e0183519. https://doi.org/10.1371/journal.pone.0183519

[40] Srinivasan L, Dutta R, Counsell SJ, Allsop JM, Boardman JP, Rutherford MA, et al. Quantification of deep gray matter in preterm infants at term-equivalent age using manual volumetry of 3-tesla magnetic resonance images. Pediatrics. 2007; 119: 759–765. https://doi.org/10.1542/peds.2006-2508

[41] Kesler SR, Reiss AL, Vohr B, Watson C, Schneider KC, Katz KH, et al. Brain volume reductions within multiple cognitive systems in male preterm children at age twelve. The Journal of Pediatrics. 2008; 152: 513–520.e1. https://doi.org/10.1016/j.jpeds.2007.08.009

[42] Schmitz-Koep B, Bäuml JG, Menegaux A, Nuttall R, Zimmermann J, Schneider SC, et al. Decreased cortical thickness mediates the relationship between premature birth and cognitive performance in adulthood. Human Brain Mapping. 2020; 41: 4952–4963. https://doi.org/10.1002/hbm.25172

[43] Klein-Flügge MC, Bongioanni A, Rushworth MFS. Medial and orbital frontal cortex in decision-making and flexible behavior. Neuron. 2022; 110: 2743–2770. https://doi.org/10.1016/j.neuron.2022.05.022

[44] Hiroshima S, Anei R, Murakami N, Kamada K. Functional localization of the supplementary motor area. Neurologia Medico-chirurgica. 2014; 54: 511–520. https://doi.org/10.2176/nmc.oa2012-0321

[45] Chang SE, Guenther FH. Involvement of the Cortico-Basal Ganglia-Thalamocortical Loop in Developmental Stuttering. Frontiers in Psychology. 2020; 10: 3088. https://doi.org/10.3389/fpsyg.2019.03088

[46] Hasson U, Chen J, Honey CJ. Hierarchical process memory: memory as an integral component of information processing. Trends in Cognitive Sciences. 2015; 19: 304–313. https://doi.org/10.1016/j.tics.2015.04.006

[47] Huntenburg JM, Bazin PL, Margulies DS. Large-Scale Gradients in Human Cortical Organization. Trends in Cognitive Sciences. 2018; 22: 21–31. https://doi.org/10.1016/j.tics.2017.11.002

[48] Euston DR, Gruber AJ, McNaughton BL. The role of medial prefrontal cortex in memory and decision making. Neuron. 2012; 76: 1057–1070. https://doi.org/10.1016/j.neuron.2012.12.002

[49] Etkin A, Egner T, Kalisch R. Emotional processing in anterior cingulate and medial prefrontal cortex. Trends in Cognitive Sciences. 2011; 15: 85–93. https://doi.org/10.1016/j.tics.2010.11.004

[50] Amodio DM, Frith CD. Meeting of minds: the medial frontal cortex and social cognition. Nature Reviews. Neuroscience. 2006; 7: 268–277. https://doi.org/10.1038/nrn1884

[51] Fair DA, Cohen AL, Power JD, Dosenbach NUF, Church JA, Miezin FM, et al. Functional brain networks develop from a "local to distributed" organization. PLoS Computational Biology. 2009; 5: e1000381. https://doi.org/10.1371/journal.pcbi.1000381

[52] Power JD, Fair DA, Schlaggar BL, Petersen SE. The development of human functional brain networks. Neuron. 2010; 67: 735–748. https://doi.org/10.1016/j.neuron.2010.08.017

[53] Supekar K, Musen M, Menon V. Development of large-scale functional brain networks in children. PLoS Biology. 2009; 7: e1000157. https://doi.org/10.1371/journal.pbio.1000157

[54] Uddin LQ, Supekar K, Menon V. Typical and atypical development of functional human brain networks: insights from resting-state FMRI. Frontiers in Systems Neuroscience. 2010; 4: 1447. https://doi.org/10.3389/fnsys.2010.00021

[55] Gao W, Alcauter S, Smith JK, Gilmore JH, Lin W. Development of human brain cortical network architecture during infancy. Brain Structure & Function. 2015; 220: 1173–1186. https://doi.org/10.1007/s00429-014-0710-3

[56] Georgieff MK. The importance of iron deficiency in pregnancy on fetal, neonatal, and infant neurodevelopmental outcomes. International Journal of Gynaecology and Obstetrics: the Official Organ of the International Federation of Gynaecology and Obstetrics. 2023; 162: 83–88. https://doi.org/10.1002/ijgo.14951

[57] Uchida Y, Kan H, Furukawa G, Onda K, Sakurai K, Takada K, et al. Relationship between brain iron dynamics and blood-brain barrier function during childhood: a quantitative magnetic resonance imaging study. Fluids and Barriers of the CNS. 2023; 20: 60. https://doi.org/10.1186/s12987-023-00464-x

[58] Uchida Y, Kan H, Sakurai K, Oishi K, Matsukawa N. Contributions of blood-brain barrier imaging to neurovascular unit pathophysiology of Alzheimer's disease and related dementias. Frontiers in Aging Neuroscience. 2023; 15: 1111448. https://doi.org/10.3389/fnagi.2023.1111448

[59] Kostović I, Jovanov-Milosević N. The development of cerebral connections during the first 20-45 weeks' gestation. Seminars in Fetal & Neonatal Medicine. 2006; 11: 415–422. https://doi.org/10.1016/j.siny.2006.07.001

[60] Smyser CD, Inder TE, Shimony JS, Hill JE, Degnan AJ, Snyder AZ, et al. Longitudinal analysis of neural network development in preterm infants. Cerebral Cortex (New York, N.Y. : 1991). 2010; 20: 2852–2862. https://doi.org/10.1093/cercor/bhq035